Received: 12 June 2020 | Revised: 16 January 2021 | Accepted: 19 January 2021

DOI: 10.1002/jccs.202000170

ARTICLE

JOURNAL OF THE CHINESE CHEMICAL SOCIETY

Imino isatin derivatives; synthesis, in silico molecular dynamic study over monoamine oxidase B, ADME prediction, and in vitro cytotoxicity evaluation

Samaneh Ahmadi[1] | **Homa Azizian**[2] | **Javad Azizian**[1]

[1]Department of Chemistry, Science and Research Branch, Islamic Azad University, Tehran, Iran

[2]Department of Medicinal Chemistry, School of Pharmacy, Iran University of Medical Sciences, Tehran, Iran

Correspondence
Javad Azizian, Department of Chemistry, Science and Research Branch, Islamic Azad University, Tehran, Iran.
Email: azizian@srbiau.ac.ir

Abstract

The monoamine oxidase B (MAO-B) depicts an attractive drug target for the development of neuro protective agents toward the treatment of neurodegenerative diseases. The current study involved synthesis, in silico and cytotoxic evaluation of N1-alkylated-5-substituted 3-imino isatin derivatives with the proposed MAO-B inhibitory activities. The In silico molecular modeling investigation was performed through the induced fit docking, molecular mechanics-generalized born surface area, and molecular dynamic method in order to uncover the binding mode interaction and their proposed impact on the active site environment and flexibility. The synthesized compounds were characterized by spectroscopic methods. Compound 3-Imino-1-pentyl indolin-2-one **(3h)** with the highest free binding energy adopts an extended conformation spanning from the flavin ring location to the entrance of the substrate cavity. In this way, Ile199 adopts the "open" conformation so the two separate cavities of MAO-B active site fused and formed a single-space, which abled the compound extending to the MAO-B entrance cavity space. From consideration of the data presented in this paper, we reveal that longer N_1-alkylated-3-imino isatin derivative could be proposed as inhibitor that would occupy both cavities of the MAO-B active site. Furthermore, the mentioned derivatives provided acceptable drug profiling based on in silico ADME calculation and MTT cytotoxicity test evaluation.

KEYWORDS

3-Imino isatin, ADME, induced fit docking, MAO-B inhibitor, MM-GBSA, molecular dynamic

1 | INTRODUCTION

Monoamine oxidase B (MAO-B) is a flavine adenine dinucleotide (FAD) dependent enzyme responsible for the oxidative deamination of endogenous neurotransmitters such as dopamine, serotonin, adrenaline, and noradrenaline along with the inactivation of exogenous aryl alkyl amines. Due to its central role in neurotransmitters metabolism, this enzyme represents an attractive drug target in age-dependent neurodegenerative diseases and its depression used for the development of neuro protective agents.[1–4]

There are many MAO-B inhibitors been developed and used as anti-Parkinson and anti-Alzheimer agent, including selegiline and rasagiline, which are known as irreversible MAO-B inhibitors.[5,6] Propargylamine moiety is a common group among the irreversible inhibitors, which covalently binds to the FAD cofactor and may

cause a serious side effect like tyramine-induced hypertensive crisis.[7,8] To overcome this problem, new generation of inhibitors, which perform through reversible MAO-B inhibition was developed. Today the only FDA approved reversible MAO-B inhibitor is safinamide used in Alzheimer disease.[9] Moreover, isatin as an endogenous small molecule (Figure 1) is described to be a reversible inhibitor of MAO enzyme,[10] which lies in the substrate cavity close to the FAD co-factor by forming hydrogen bonding with the conserved water molecules.[11] In this regard, some isatin-based compounds are shown to possess MAO-B inhibition activity.[12,13] In addition, the —N═CH— linkage, is well known as a building block in organic synthesis evaluated for different kinds of biological activity such as antimicrobial, antifungal, anti-inflammatory, anti-cancer, antitumor, and herbicidal.[14,15] Schiff bases of isatin were reported to possess anti-HIV,[16,17] anticonvulsant,[18] antibacterial,[19–22] antiprotozoal,[23,24] antifungal,[25–27] antiviral,[28–30] and antituberculosis[31–33] activity.

Based on these facts, we decided to synthesize 3-imino indolin-2-one derivatives for their biological evaluation. Previously, the synthesis of 3-imino indolin-2-one derivatives was carried out using a different kind of solvents under refluxing conditions.[34–37] In the current study, the use of solvent has been avoided and the reactions were carried out in the presence of an acid catalyst process (Scheme 1). While the evolution of biological activities of the synthesized compounds is currently ongoing, the cytotoxicity of compounds was assessed in order to reveal the safety profile of these compounds.

Moreover, the extensive in silico molecular modeling investigation was performed through the series of computational methods. At the beginning, the induced fit docking (IFD) protocol used to uncover the binding mode interaction of the synthesized compounds over the 5 Å distance around the MAO-B active site. Thereafter, molecular mechanics-generalized born surface area (MM-GBSA) calculation was performed based on the best posed structure obtained from the IFD complexes to calculate the relative free energy, which reflect the ligand-binding affinity. Finally, molecular dynamic method was achieved over the ligands with the highest ligand-binding energy in order to investigate the active site structures and environment flexibility based on the best-proposed compounds interaction over the MAO-B enzyme.

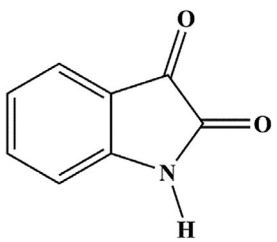

FIGURE 1 Representation of isatin structure

2 | RESULTS AND DISCUSSION

2.1 | Reliability of the IFD protocol

Cross docking is known as an accurate method for the root mean square deviation (RMSD) validity of docking protocol.[15] The applied docking procedure reliability was validated by cross docking of several known crystallographic MAO-B inhibitors over 2v5z. First, all the available crystallographic structures were aligned over 2v5z structure. Then the crystallographic ligands were docked into 2v5z and the docked conformations corresponding to the lowest IFD Score were selected as the most possible binding modes. The RMSD was calculated for each ligand to measure the docking prediction accuracy (Table 1). The pose was considered optimal if its RMSD found to be less than 2 Å.[38,39] The RMSD of the re-docked conformations of safinamide over 2v5z was obtained to be 0.40 Å, which is considered successfully docked.

The MAO B active site made of two cavities, the substrate cavity ahead of the flavin as cofactor and the entrance cavity lied underneath the protein surface, which blocked by a loop consists of residues 99–112.[40]

Docking of safinamide over the MAO-B active site showed that it bonded in front of flavin cofactor and occupied both the substrate and entrance cavity space (Figure 2). The propanamide group of the syfinamide lied in the aromatic cage (showed in yellow stick) formed by Tyr398 and Tyr435 and interacted with Gln206 and Tyr435 through H-bond and water mediated H-bond, respectively. In addition, the middle benzyl group stabilized with Phe326 at the substrate cavity through π-π stacking interaction (showed in orange stick). Finally, the end part of safinamide, the fluorophenyl moiety, extended toward the entrance cavity of the MAO-B enzyme, which surrounded by Ile199, Ile316, and Phe103 through Van der Waals interactions (showed in purple). As a result, the validity of docking parameters was reasonable in order to predict the pose of other investigated structures.

2.2 | Investigating IFD interaction of the synthesized compounds

The performed docking procedure was then applied to evaluate the interaction between newly synthetized

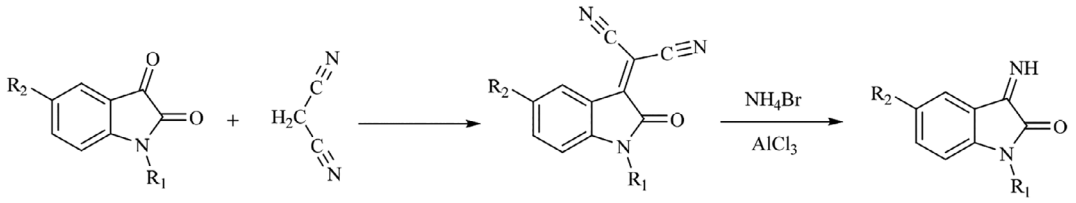

SCHEME 1 Preparation of 3-imino indolin-2-one

TABLE 1 The ligands root mean square deviation (RMSD) values of the docked and crystalized forms over monoamine oxidase B

No.	PDB id	Co-crystalized ligand	Resolution (Å)	RMSD (Å)
1	2v5z	Safinamide	1.6	0.12
2	2c67	Rasagiline	1.7	0.40
3	1oja	Isatin	1.7	0.54
4	2byb	Selegiline	2.2	0.65
5	2vz2	Mofegilide	2.3	0.43

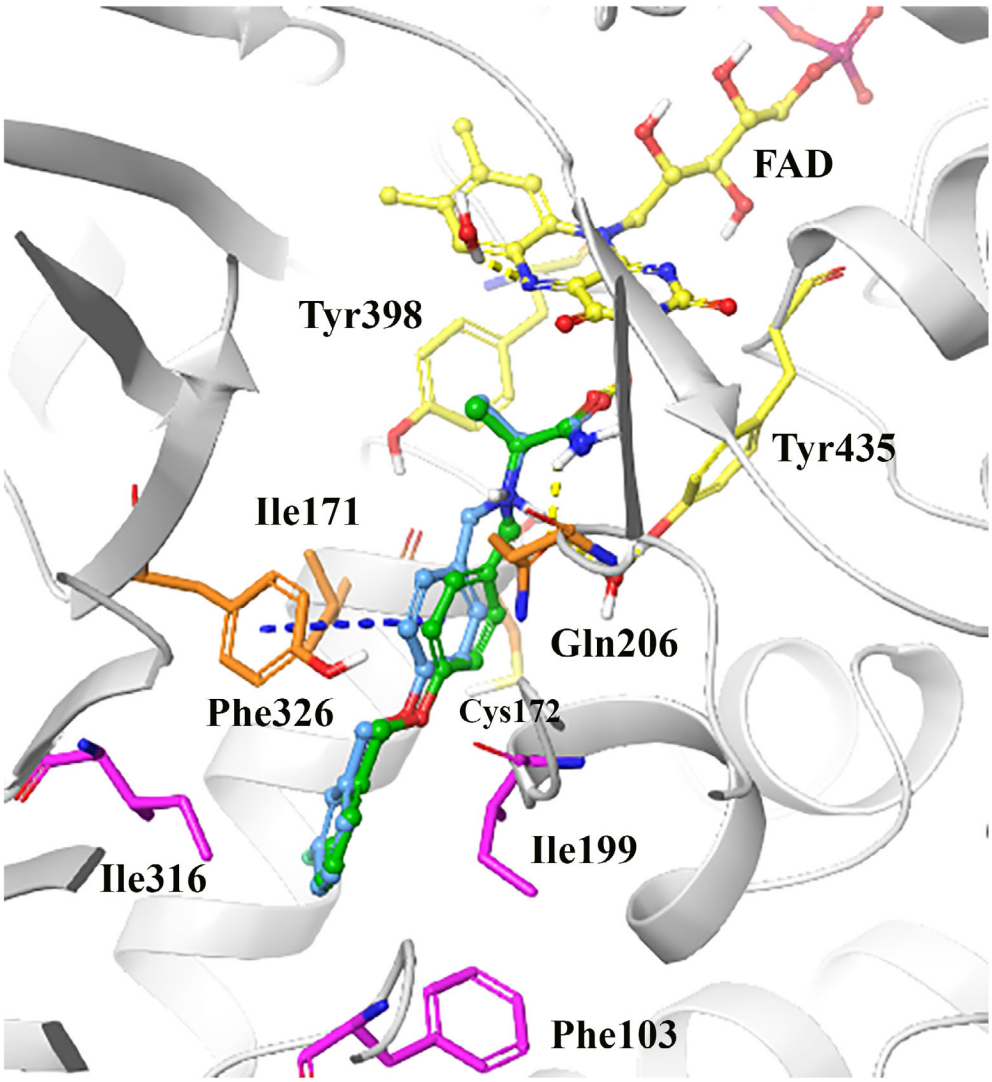

FIGURE 2 Close-up representation of binding interactions of the superposed docked (cyan) and co-crystalized safinamide (green) over monoamine oxidase
B. Structural waters and their H-bond interaction render in stick. Aromatic cage, substrate cavity, and entrance cavity residues colored in yellow, orange, and pink, respectively

compounds (**3a–3i)** over the MAO-B active site in comparison to the reference MAO-B inhibitors. The top scoring pose of all compounds was selected based on IFD Score and was analyzed for pose investigation and free binding energy calculation using Prime MM-GBSA method.

Table 2 shows all of the synthesized isatin analogs have better glide energy than the mentioned reference inhibitor except that of safinamide. In addition, it has been shown that except compounds **3a** all the synthesize compounds have higher free binding energy than isatin (known as a reversible noncovalent MAO-B inhibitor).[11] By comparing the values mentioned under the MM-GBSA column, compounds **3b**, **3c**, **3g**, **3h**, and **3i** have higher free binding energy than selegiline. This result proposed that isatin analogs have good binding affinity for the active site of MAO-B enzyme.

Figure 3a depicts that the polar imino-2-oxoindole ring of isatin (colored in green) and compounds **3a**, **3b**, **3c**, **3d**, and **3e** lied in the substrate cavity (colored in orange) and pointed toward flavin ring at the aromatic cage (colored in yellow) in a perpendicular manner, which observed for the most MAO-B-inhibitor complexes[11] and the rest of the structures involved in van der Waals contacts with hydrophobic residues of the substrate cavity space.

Furthermore, docking pose of the compounds **3g** and **3h** with N_1-alkyl substitution over MAO-B active site indicates that the aromatic ring of the compounds adopts the same orientation and position as isatin except the N_1-alkyl groups, which are extended through the entrance cavity space (colored in pink), and caused increasing the free binding energy of the mentioned compounds (Figure 3b). Comparing the free binding energies of the mentioned compounds reveal that increasing the length of the N_1-alkyl chain from ethyl to butyl (**3g** and **3h)** increase the MM-GBSA value as a result of expanding the contact area over the entrance cavity (Table 2, highlighted in yellow).

Among the synthesized compounds, the free binding energy of compound **3h** was noticed to be the highest one with the value of −45.69 kcal/mol, which was higher than standard inhibitors; isatin, selegiline, and mofegiline (−28.29, −38.67, and −44.20 kcal/mol, respectively).

TABLE 2 Glide energy and free binding energy (kcal/mol) of the synthesized compounds over monoamine oxidase B (pdb id = 2v5z)

No	Glide energy	Molecular mechanics-generalized born surface area (kcal/mol)
3a	−30.378	−20.67
3b	−30.855	−39.25
3c	−35.205	−39.30
3d	−35.100	−37.08
3e	−34.147	−33.44
3f	−33.007	−30.56
3g	−33.450	−40.68
3h	−42.055	−45.69
3i	−36.164	−38.84
Isatin	−30.300	−28.29
Selegilin	−30.787	−38.67
Rasagilin	−30.284	−56.47
Mofegiline	−30.423	−44.20
Safinamide	−55.362	−166.7

2.3 | Molecular dynamic simulation

In order to understand the criteria for rational designing of the MAO-B inhibitors, it is necessary to uncover the structural perturbations incurred by the compound with the highest free binding energy (compound **3h**) over MAO-B active site (pdb id = 2v5z) and compare the effect of this compound on the active site environment in comparison to selegiline, which is known as the old FDA approved drug used as anti-Parkinson and anti-Alzheimer agent.

RMSD of the protein's Cα from its initial to final conformation was applied over 20 ns of the MD simulation in order to study the stability of the protein-ligand complex. The RMSD simulation showed that the MAO-B complexed with selegiline maintained an overall stability after 2n of the MD simulation time with higher fluctuation stabilizing at an average of 2.75 Å (Figure 4, blue line), while the bounded-state of compound **3h** displayed longer equilibration time with obviously maximum fluctuation value around 2 Å (Figure 4, red line). The RMSD value of each MAO-B ligand complex indicates that the employed simulation time has been enough to obtain an equilibrium structure over the simulation time (Figure 4). Thus, the structures at the MD equilibrium state used to investigate the structural specificity of the ligand-protein complexes.

Furthermore, root-mean-square fluctuation (RMSF) of MAO-B was examined in the bounded-state enzyme with selegiline and compound **3h** (Figure 5). It is observed that both compounds provided the same structural flexibility pattern through the MAO-B enzyme structure in the presence of FAD cofactor except for the terminal residues. According to the result, the mentioned

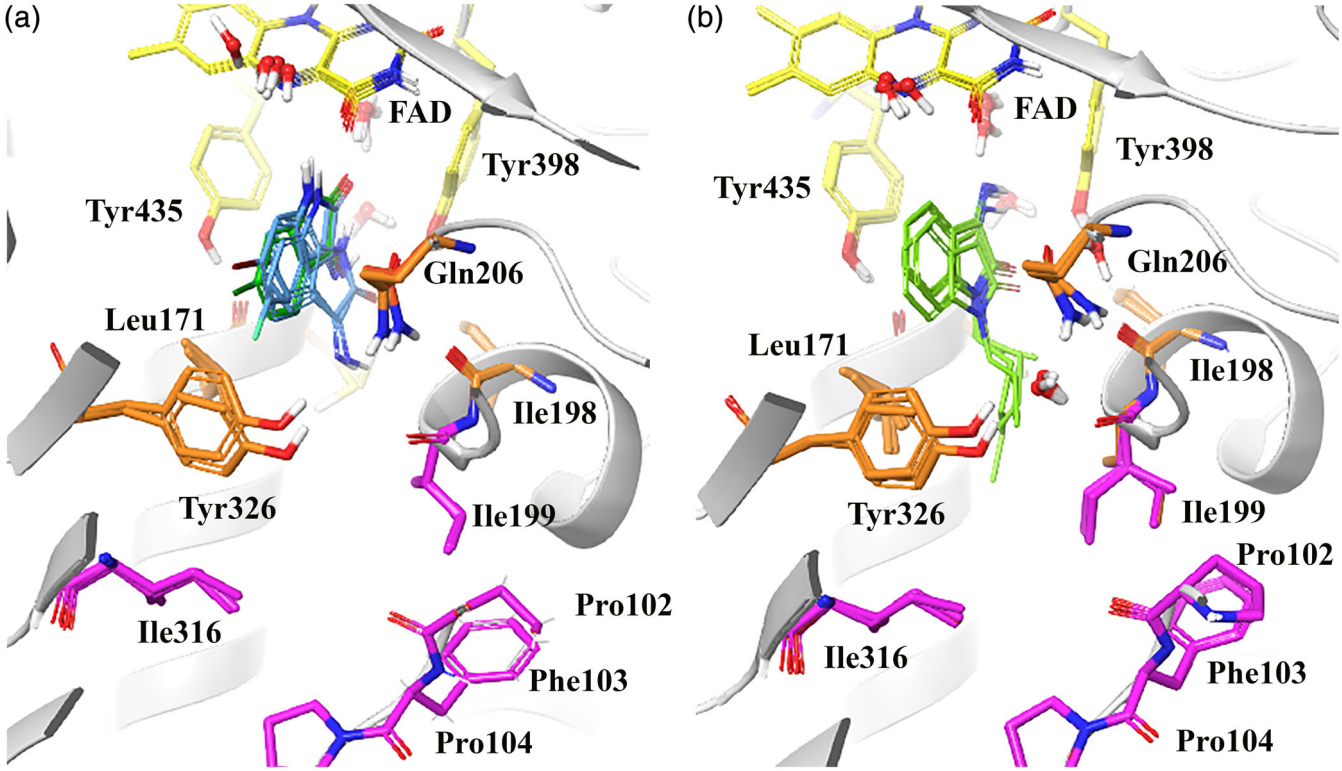

FIGURE 3 Close-up representation of synthesized compound over monoamine oxidase B active site, (a) induced fit docking (IFD) pose of compounds isatin (colored in green), **3a**, **3b**, **3c**, **3d**, and **3e** (colored in cyan), which do not have N_1-alkyl substitution, (b) IFD pose of compounds **3g**, and **3h** with N_1-alkyl substitution (colored in light green). Aromatic cage, substrate cavity, and entrance cavity residues colored in yellow, orange, and purple, respectively

FIGURE 4 Root mean square deviation of the monoamine oxidase B Cα in complexed with selegiline (in blue) and compound **3h** (in red) for over 20 ns of the MD simulation time

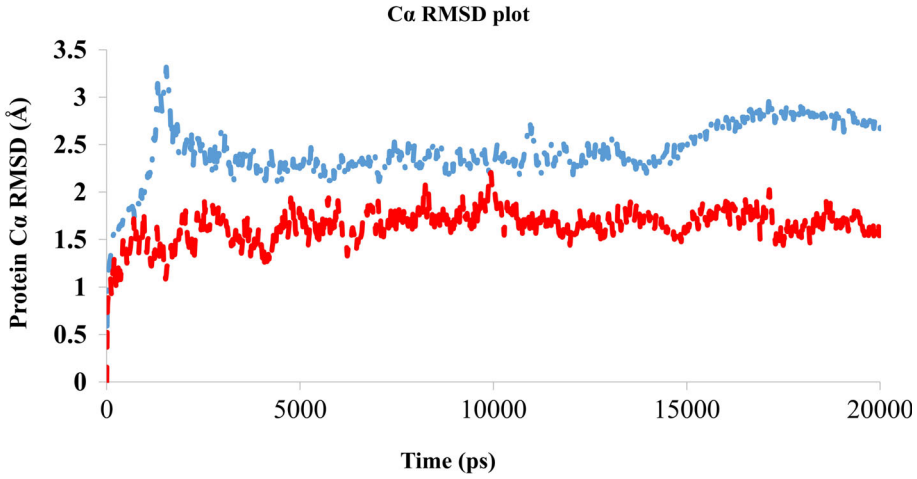

lower RMSF value occurs upon ligand binding to the enzyme as a result of non-bonding interaction between the ligand and the enzyme active site.

The molecular interactions of selegiline and compound **3h** over the binding site of MAO-B involve a number of hydrophilic and van der Waals contacts with the active side surrounded residues, which are schematically shown in Figure 6. There are four ordered water molecules inside the cavity located at the substrate cavity and aromatic cage, which contribute to the inhibitor interactions.

Figure 6a shows that selegiline bonded to human MAO-B active site occupying substrate cavity in which the amino alkyne group formed two water-mediated H-bond through its amino group with Tyr435 located at aromatic cage and Gln206 over the second part of MD simulation with the occupancy time of 44 and 39%, respectively. In addition, the aromatic ring stabilized

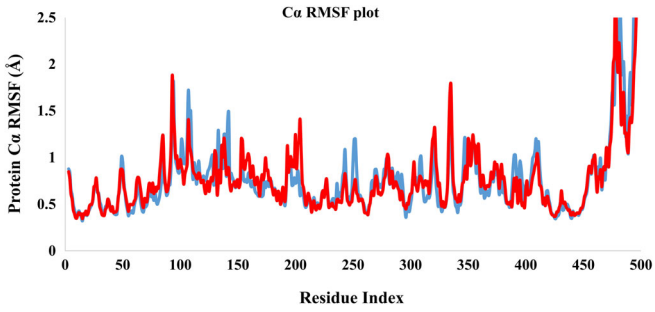

FIGURE 5 Root-mean-square fluctuation of the monoamine oxidase B Cα in complex with selegiline (colored in blue) and compounds **3h** (colored in red) for over 20 ns of the MD simulation time

with hydrophobic residues include Tyr326, Phe168, and Ile 171 located at the line of substrate cavity for about the whole MD simulation time.

On the other way, Figure 6b shows imino group of compound **3h** stabilized through the MAO-B active site by forming H-bond interaction with Tyr435 the same as selegiline tertiary amine, except that the mentioned interaction persisted for the higher MD simulation time (84%). This structural finding consistent with the idea that the aromatic cage plays an important role as a recognition site for the amine group of the inhibitors.[41]

Furthermore, compound **3h** interacted through hydrophobic interaction with Lue171 and Cys172 located at the top of the substrate cavity for about the first 12 ns of MD simulation time, while the mentioned interactions were disappeared and substituted by hydrophilic water-mediated H-bonding with Arg197 and His200, which lied at the separating loop for the rest of the MD simulation time (with high occupancy time).

Furthermore, we study the active site cavity shape alongside the interaction mode of the N_1-alkylated group of compound **3h** during the MD simulation time. For this purpose, the distances between Ile199 and Tyr326 located near the junction of the entrance and substrate cavities in two opposite side are recorded and analyzed.

In previous study, it was found that Ile199, located near the junction of the entrance and substrate cavities,

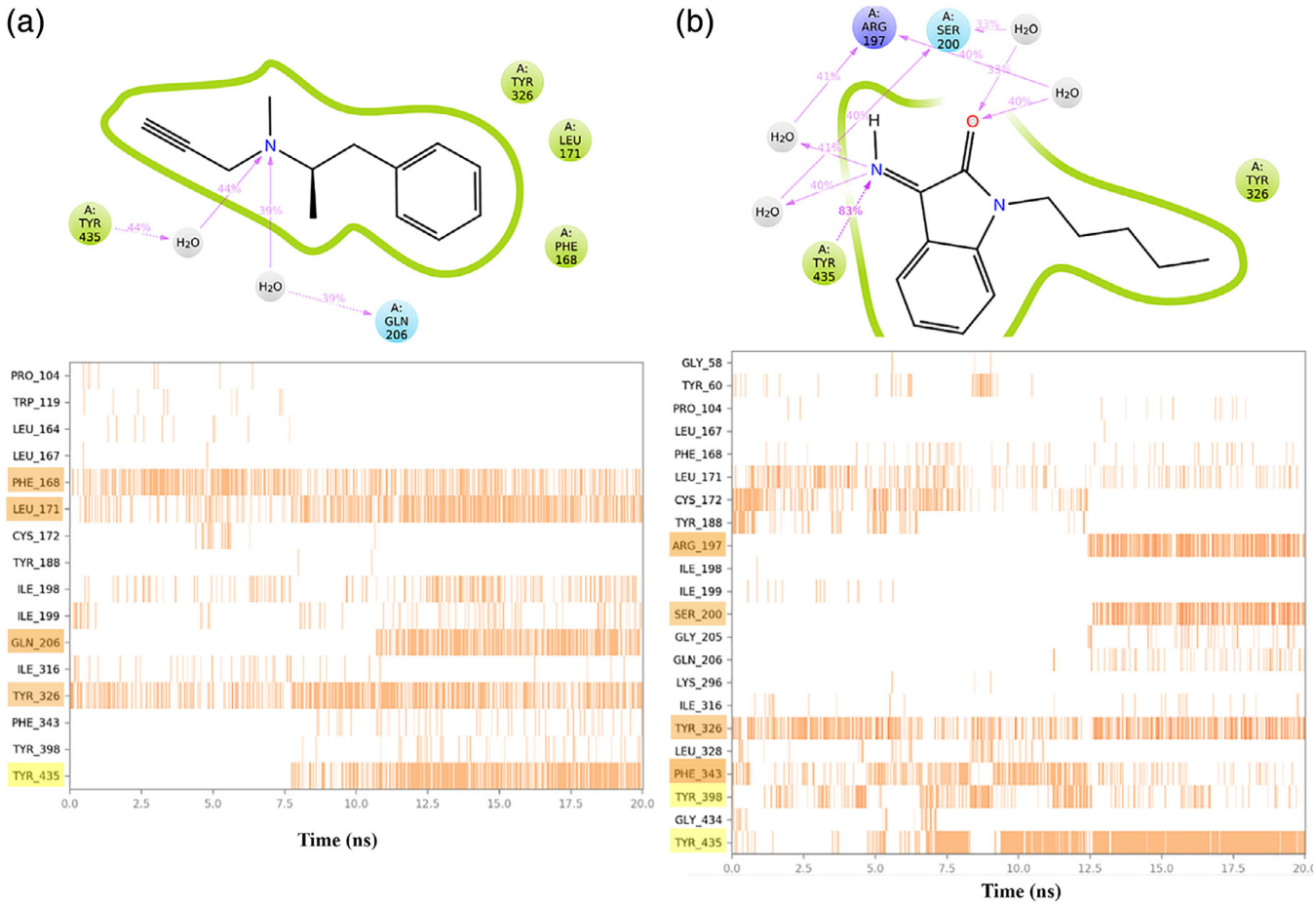

FIGURE 6 2D (up row) and timeline (below row) representation of ligand-residue interactions that occur during the simulation time, which include monoamine oxidase B bound-state of selegiline (a) and compound **3h** (b), respectively. Aromatic cage and substrate cavity residues highlighted in yellow and orange, respectively

engaged in two different conformers relative to the MAO-B active site cavity; the first one is a "closed conformation" in which its side chain pointed toward the active site cavity space and the next one is an "open conformation" merging the two cavities.[11]

Figure 7a displays the distance between Tyr326 (Cα) and Ile199 (C_{CD1}) over the MAO-B bound-state during the 20 ns of simulation time. In the case of compound **3h** bound-state, the separation of the mentioned residues at the beginning of the simulation time was about 9.5 Å and significantly increased up to 17 Å during the 10 ns followed by gradually decreased to about 15 Å in the next 4 ns and finally stabilized until the rest of the simulation time (the red line). On the other hand, in the case of selegiline bound-state, after a sharp increasing the specified distance decreased step by step to about below the 11 Å after 14 ns and equilibrated up to the end of simulation time (the blue line).

In order to investigate Ile199 conformers along the simulation time, three snapshots of the enzyme bound-states to compound **3h** and selegiline provided at the beginning, middle, and the end of simulation time (the black dash-lines in Figure 7b,c). Snapshots related to the enzyme complexed with compound **3h** depict that Ile199 side chain was along the wall of the active site, which corresponds to the open conformer, while in the case of selegiline bound-state, the mentioned residue side chain rotated toward the active site cavity, which

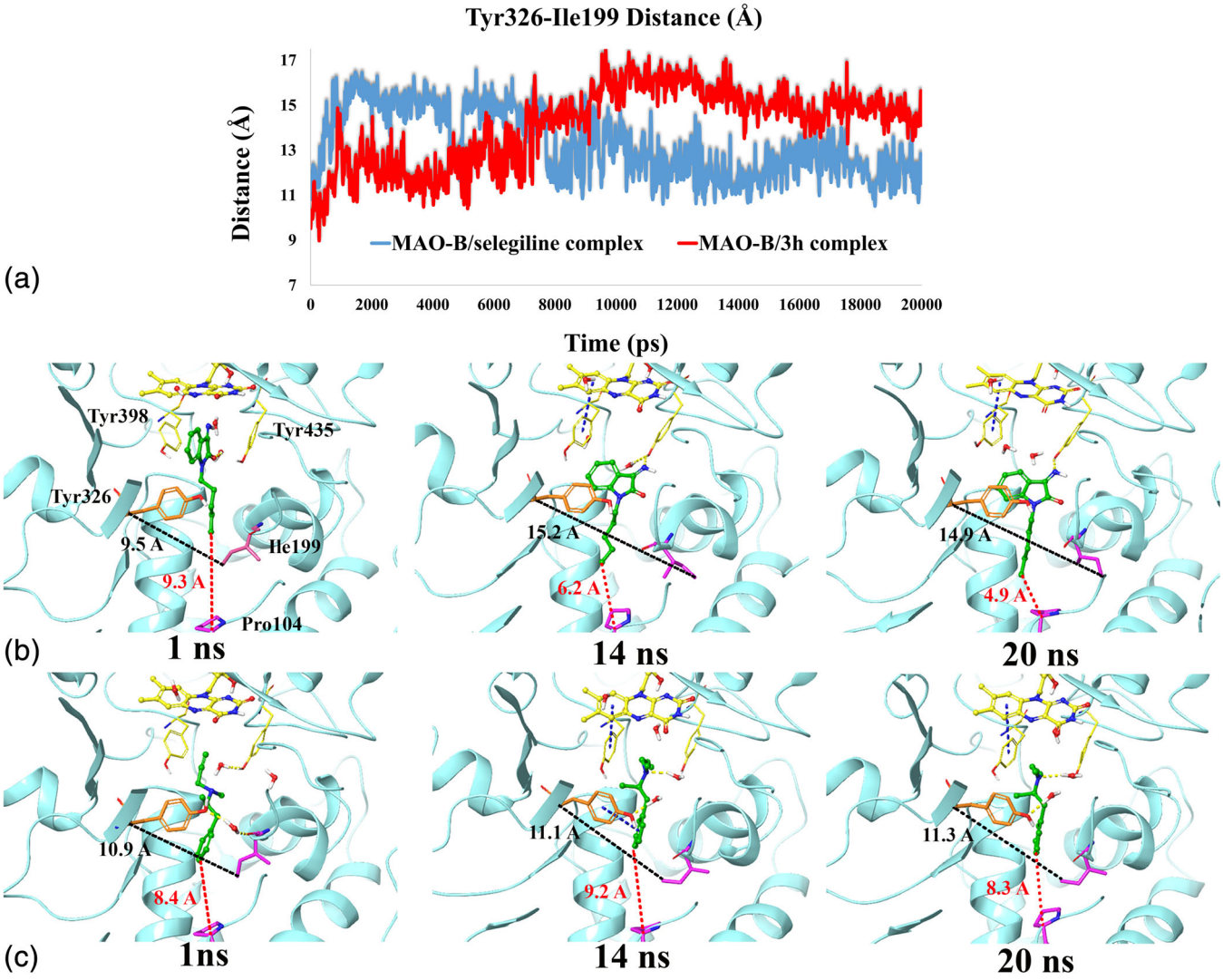

FIGURE 7 MD simulated distance between Tyr326 (Cα)–Ile199 (CCD1) in selegiline (blue) and compound **3h** (red) in monoamine oxidase B bound-state (a). Representative snapshots from MD simulations of compound **3h** (b) and selegiline (c) focusing on Ile199 conformations (open/close), distance between Tyr326 (Cα) and Ile199 (CCD1) (showed in black dash-line), and the distance between the tail of compound and Pro104 (Cα) (showed in red dash-line). Aromatic cage, substrate cavity, and entrance cavity residues colored in yellow, orange, and purple, respectively

correlates to the close rotamer. The conformer of Ile199 affects the structural shape of the active site in the way that the open conformer merged both of the substrate and entrance cavity and formed a single space active site, whereas the close conformer divided the active site area by separating these two-cavity space.

Furthermore, analyzing the distance between Pro104 (Cα) located at the active site closing loop and the tail part of the bound-state compounds depicts the extent of ligand penetration into the active site from the entrance space to the substrate cavity pocket. In the case of compound **3h**, the mentioned distance decreased from 9.3 Å at the begin to 4.9 Å at the end of simulation time, while in the case of selegiline it oscillated within 8.5 Å because of steric clash of the bottom part of selegiline phenyl ring with Ile199 side chain (Figure 7b,c, the pink dash-lines).

In summary, according to the compound **3h** bounding-state, Ile199 is in open rotamer conformation so the two-cavity fused forming a single space, which abled the N_1-pentyl extending to the MAO-B entrance cavity space. This finding proposed that N_1-alkylated-3-iminoisatin could be considered a new reversible inhibitor that would occupy both cavities of the MAO-B active site.

2.4 | In silico ADME properties of synthesized compounds

The important pharmacokinetic properties of the synthesized compounds, which represent drug- likeness, metabolism, BBB transportation, and bioavailability, were calculated with QikProp module of Schrodinger. Based on the "Lipinski rule of five" distributions of the compound molecular weights, calculated lipophilicity (log P), number of hydrogen bond acceptors, number of hydrogen bond donors, number of rotatable bonds, and the number of violations of Lipinski's rule of five were used to assess the "drug-likeness" of the synthesized compounds. According to Table 3, it was observed that all Lipinski rules were in acceptable value and the synthesized compounds showed no Lipinski violations, which indicates a high probability of finding drug-like potential within these series.

Furthermore, The blood brain barrier (BBB) absorption in turn relays on the solubility, oral absorption, and BBB permeability of the compound. The computed parameters were used to assess oral absorption, including the predicted aqueous solubility (log Swat), the predicted % human oral absorption (%HOA), and the predicted brain/blood partition coefficient (Table 4). According to Table 4, it was observed that all of the predicted descriptors are in acceptable value, which indicates the synthesized compounds have adequate BBB bioavailability so they could emerge good candidate for drug discovery.

2.5 | Cytotoxicity assay

Toxicity is one of the most important reason for failure of new drug entry into the pharmaceutical market. Therefore, cytotoxicity test is very important filtering stage for accepting a drug candidate. Figure 8 shows MTT cytotoxic activity of compounds **3a**–**3i** against both NIH/3T3 and MCF-7 cells. Our result indicates the IC_{50} values of the synthesized compounds were >1,000 μM against both NIH/3T3 and MCF-7 cells during 24 and 48 hr, which means the synthesized compounds showed neither

TABLE 3 The Lipinski-rule of five properties of investigated compounds

No.	Molecular weight	HBD[a]	HBA[b]	Log *P* o/w[c]	Rotor[d]	ROF[e]
3a	146.148	2	3.5	1.298	1	0
3b	180.593	2	3.5	1.665	1	0
3c	225.044	2	3.5	1.472	1	0
3d	191.146	2	4.5	−0.469	2	0
3e	160.175	2	3.5	1.108	1	0
3f	160.175	1	4	0.878	1	0
3g	174.202	1	4	1.032	2	0
3h	216.282	1	4	2.187	5	0
3i	174.202	1	3.5	1.392	2	0

Abbreviations: HBA, hydrogen bond acceptors; HBD, hydrogen bond donors; ROF, rule of five.

[a]Number of average hydrogen bond donor (recommended value 0.0–6.0).

[b]Number of average hydrogen bond acceptor (recommended value 2.0–20.0).

[c]Predicted octanol/water partition co-efficient (acceptable range from −2 to 6.5).

[d]Number of rotatable bond (recommended value 2.0–20.0).

[e]Number of violations of Lipinski's rule of five (maximum 4).

TABLE 4 The calculated ADME properties of synthesized compounds

No.	Log S_{wat}[a]	PlogBB[b]	% HOA[c]	Metab[d]	RO3[e]
3a	−1.391	−0.622	81.400	0	0
3b	−1.925	−0.479	83.549	0	0
3c	−1.951	−1.134	82.416	0	0
3d	−1.507	−0.676	54.491	1	0
3e	−1.581	−0.344	80.291	1	0
3f	−1.897	−0.379	85.323	0	0
3g	−1.861	−0.463	87.139	0	0
3h	−2.939	−0.396	93.933	0	0
3i	−2.152	−0.417	89.490	0	0

Abbreviation: HOA, human oral absorption.
[a]Predicted aqueous solubility in mol/dm^3 (−6.5 to 0.5) (QPlogS >−5.7).
[b]Predicted brain/blood partition coefficient (acceptable range: −3.0 to 1.2).
[c]Percentage human oral absorption (<25% is poor and >80% is high).
[d]Number of likely metabolic reactions (primary metabolites <7).
[e]Number of violations of Jorgensen's rule of three. Compounds with fewer (preferably no) violations of these rules are more likely to be orally available.

cytotoxicity toward normal tissue cells nor cancerous one. Having low toxicity is very important character for any drug candidate.

3 | EXPERIMENTAL

3.1 | Chemistry

All reagents were purchased from Sigma Aldrich Company (Tehran, Iran). All chemicals were reagent grade and were without further purification. Melting points were detected with an Electrothermal 9300 apparatus (Ontario, Canada). ^{1}H-NMR and ^{13}C-NMR spectra were obtained by a Brucker AVANCE 500 Ultra shield Spectrometer (Brucker, Rheinstetten, Germany). Tetramethylsilane used as an internal standard. The IR spectra were obtained using Jasco FT-IR-410 spectrophotometer (KBr disks). Mass spectra were obtained using a Finnigan

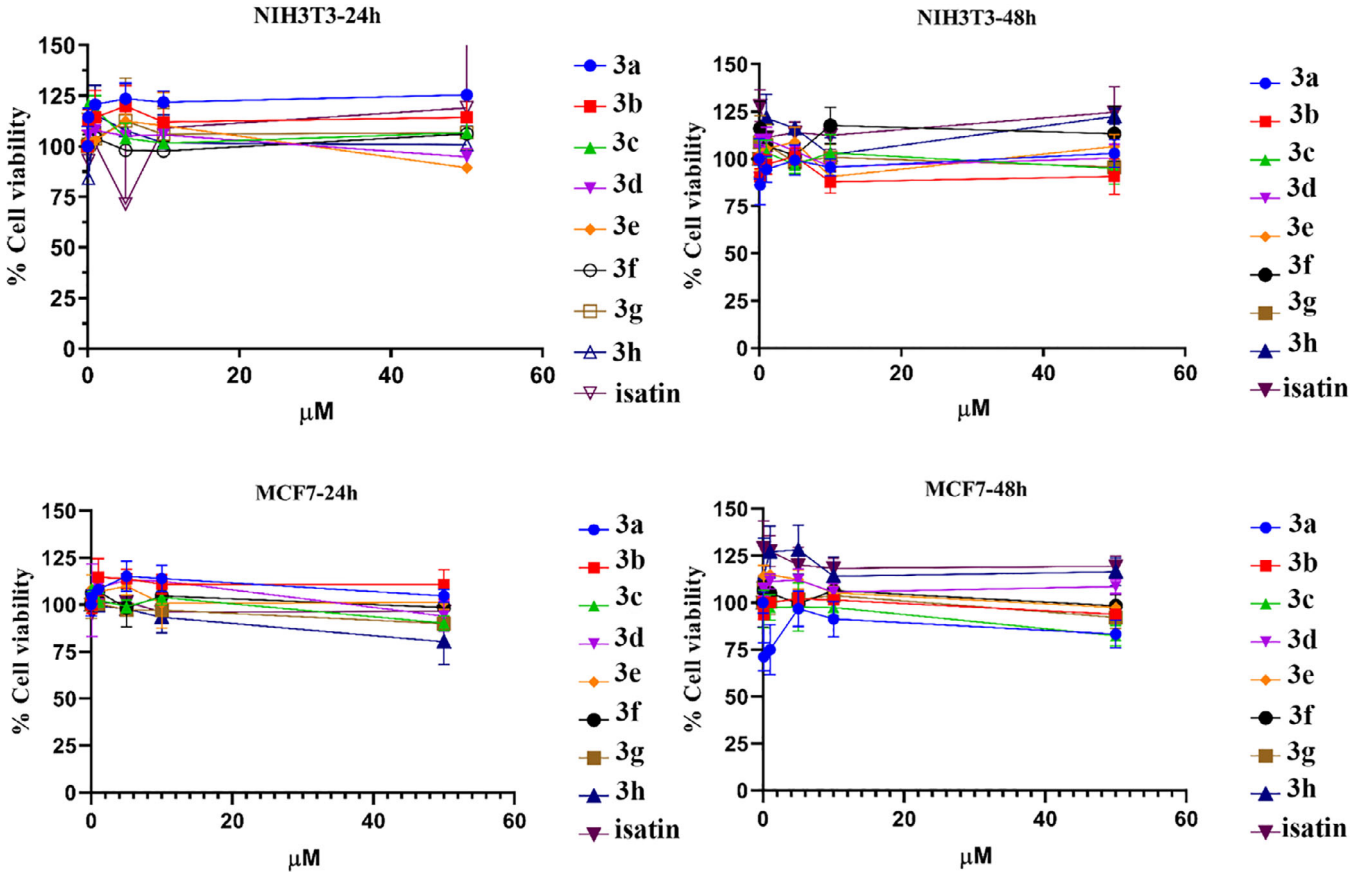

FIGURE 8 Viability test of the synthesized compounds on NIH3T3 and MCF-7 cells after 24 and 48 hr by MTT assay. Percentage of live cells was calculated relative to control group. Values are presented as mean ± SD of five independent experiments

Mat TSQ-70 spectrometer at 70 eV (Finnigan Mat, Bremen, Germany).

3.2 | Preparation of 3-imino indolin-2-one derivatives

The syntheses of N_1-alkylated-5-substituted isatin have been done according to the previously published article.[42] A mixture of N_1-alkyl-5-substituted isatins (0.1 mmol) and malononitrile (0.1 mmol) stirred at room temperature for 15 min. Then after, $AlCl_3$ (0.01 mol) added to the reaction mixture, and heated up to 100°C. In continue, ammonium bromide (0.1 mol) added, stirred, and heated at 100°C for about 2 hr (for synthesizing compound **3L**, ethylamine was used). The process followed by cooling the mixture, adding NaOH 10%, and diluting with DCM. The organic layer washed with water, dried on Na_2SO_4, and evaporated. Finally, the compounds crystallized from ethanol and the purity of the compounds was monitored by thin layer chromatography. The melting points and yields reported in Table 5. The structures of the products were confirmed by elemental and spectral analysis as follows and on supplementary material.

3.2.1 | 3-imino indolin-2-one (3a)

Brown solid. Yield 90%, MP: 142–143°C. IR (KBr) cm^{-1}: 3,473.09 (NH), 3,348.77 (NH), 3,028.49 (Ar), 1,625.35 (CO, CN), 1,428.7 (C═C). ^{1}HNMR (δ, DMSO-d6): 11.13 (1H, s, NH), 6.69 (1H, d, J = 7.8 Hz, Ar), 7.17 (1H, t, J = 7.4 Hz, Ar), 6.46 (1H, d, J = 8.1 Hz, Ar), 7.52 (1H, t, J = 8.1 Hz, Ar), 7.04 (1H, s, NH). ^{13}CNMR (δ, DMSO_d6): 197.1, 169.1, 150.7, 133.6, 133.0, 114.3, 113.0, 112.9. MS (ESI, 70 eV) *m/z* (%): 146.05 (100), 147.05 (8.7). Elemental Analysis for $C_8H_6N_2O$: C, 65; H, 4.1; N, 20.5; O, 10.9.

3.2.2 | 5-Chloro-3-imino indolin-2-one (3b)

Yield 92%; IR (KBr) cm^{-1}: 3,428.47, 3,428.47 (NH), 641.94 (CO), 1,517.89 (CN), 1,457.92 (C═C), 657.80 (C—Cl). ^{1}HNMR (δ, DMSO-d6): 11.13 (1H, s, NH), 8.23 (1H, s, NH), 7.95 (1H, dd, Ar), 7.62 (1H, d, Ar), 7.55 (1H, s, Ar). ^{13}CNMR (δ, DMSO-d6): 169.4, 144.4, 132.0, 124.6, 124.0, 115.0, 113.9. MS (ESI, 70 eV) *m/z* (%): 180.01 (100), 182.01 (32), 181.01 (8.7), 183.01 (2.8). Elemental Analysis for $C_8H_5ClN_2O$: C, 53.33; H, 2.77; Cl, 19.72;N, 16.66; O, 8.88.

3.2.3 | 5-Bromo-3-imino indolin-2-one (3c)

Yield 93%. IR (KBr) cm^{-1}: 3,444.7, 3,444.7 (NH), 1,619.90 (CO, CN), 1,428.15 (C═C), 882.32 (C—Br). ^{1}HNMR (δ, DMSO-d6): 11.22 (1H, s, NH), 8.36 (1H, s, NH), 7.72 (1H, dd, Ar), 7.76 (1H, d, Ar), 7.74 (1H, s, Ar). ^{13}CNMR (δ, DMSO-d6): 116.8, 122.2, 125.8, 129.6, 133.0, 145.1, 166.8,

TABLE 5 Physico-chemical properties of the synthesized compounds (**3a–3i**)

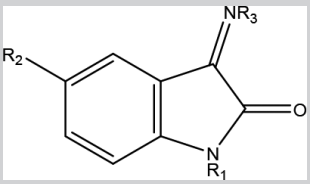

Entry	Molecular weight	R_1	R_2	R_3	m.p. (°C)	Yield (%)	Molecular formula
3a	146.05	H	H	H	142	90	$C_8H_6N_2O$
3b	180.01	H	Cl	H	225	92	$C_8H_5ClN_2O$
3c	223.96	H	Br	H	253	93	$C_8H_5BrN_2O$
3d	191.03	H	NO_2	H	281	95	$C_8H_6N_3O_3$
3e	160.06	H	CH_3	H	210	90	$C_9H_8N_2O$
3f	160.06	CH_3	H	H	186	75	$C_9H_8N_2O$
3g	174.08	C_2H_5	H	H	208	73	$C_{10}H_{10}N_2O$
3h	216.03	C_4H_{11}	H	H	277	65	$C_{13}H_{16}N_2O$
3i	174.08	H	H	C_2H_5	229	80	$C_{10}H_{10}N_2O$

171.2. MS (ESI, 70 eV) *m/z* (%): 223.96 (100), 225.96 (97), 224.96 (8.7), 226.96 (8.4). Elemental Analysis for $C_8H_5BrN_2O$: C, 42.86; H, 2.23; Br, 35.27; N, 13.39; O, 7.14.

3.2.4 | 3-Imino-5-nitro indolin-2-one (3d)

Yield 95%. IR (KBr) cm^{-1}: 3,435.09, 3,554.09 (NH), 1,642.73 (CO), 1,445.90 (C═C), 1,313.20, 1,569.84 (NO_2). ^{1}HNMR (δ, DMSO-d6): 11.79 (1H, s, NH), 8.45 (1H, s, NH), 8.37 (1H, dd, Ar), 8.17 (1H, d, Ar), 8.21 (1H, s, Ar). ^{13}CNMR (δ, DMSO-d6): 174.5, 149.8, 148.9, 141.1, 138.1, 135.7, 118.4, 111.5. MS (ESI, 70 eV) *m/z* (%): 191.03 (100), 192.04 (8.7). Elemental Analysis for $C_8H_6N_3O_3$: C, 50.25; H, 3.14; N, 23.55; O, 25.12.

3.2.5 | 3-Imino-5-methyl indolin-2-one (3e)

Yield 90%. IR (KBr) cm^{-1}: 3,473.09, 3,340.77 (NH), 3,020.49 (Ar), 2,970.12 (CH), 1,620.35 (CO,CN), 1,428.7 (C═C): ^{1}HNMR (δ, DMSO-d6): 11.23 (1H, s, NH), 7.41 (1H, s, NH), 7.33 (1H, dd, Ar), 7.14 (1H, d, Ar), 6.82 (1H, s, Ar), 2.23 (3H, s, CH_3). ^{13}CNMR (δ, DMSO-d6): 187.9, 157.0, 131.8, 130.9, 125.7, 118.4, 111.5, 14.3. MS (ESI, 70 eV) *m/z* (%): 160.06 (100), 161.07 (9.7). Elemental Analysis for $C_9H_8N_2O$: C, 67.47; H, 4.99; N, 18.74; O, 9.99.

3.2.6 | 3-Imino-1-methyl indolin-2-one (3f)

Yield 75%. IR (KBr) cm^{-1}: 2,921.89 (CH), 3,442.50 (NH), 1,637.72 (CO, CN), 1,455.19 (C═C). ^{1}HNMR (δ, DMSO-d6): 8.23 (1H, s, NH), 7.95 (1H, dd, Ar), 7.62 (1H, dd, Ar), 7.60 (1H, d, Ar), 7.55 (1H, d, Ar), 3.55 (3H, s, CH_3). ^{13}CNMR (δ, DMSO-d6): 166.8, 159.8, 151.2, 138.8, 124.9, 123.0, 118.3, 113.8, 55.8. Elemental Analysis for $C_9H_8N_2O$: C, 67.47; H, 4.99; N, 18.74; O, 9.99.

3.2.7 | 1-Ethyl-3-imino indolin-2-one (3g)

Yield 73%. IR (KBr) cm^{-1}: 2,970.63, 2,872.96 (CH), 3,471.92 (NH), 1,613.40 (CO, CN), 1,444.41 (C═C). ^{1}HNMR (δ, DMSO-d6): 8.00 (1H, s, NH), 7.68 (1H, d, J = 8.0 Hz, Ar), 7.64 (1H, t, Ar), 7.14 (1H, d, J = 8.0 Hz, Ar), 7.10 (1H, t, H), 2.89 (2H, q, CH_2), 0.89 (3H, t, CH_3). ^{13}CNMR (δ, DMSO-d6): 25.7, 41.3, 111.5, 118.4, 130.9, 131.8, 135.4, 138.4, 159.2, 163.0. Elemental Analysis for $C_{10}H_{10}N_2O$: C, 68.93; H, 5.71; N, 17.23; O, 9.19.

3.2.8 | 3-Imino-1-pentyl indolin-2-one (3h)

Yield 65%. IR (KBr) cm^{-1}: 3,430.20 (CH), 3,443.5 (NH), 1,642.61 (CO, CN), 1,387.78 (C═C). 1,428.77. ^{1}HNMR (δ, DMSO-d6). 7.04 (1H, s, NH), 6.69 (1H, d, J = 8.0 Hz, Ar), 7.17 (1H, t, Ar), 6.46 (1H, t, Ar), 7.5198 (1H, d, J = 8.0 Hz, Ar), 2.89–0.9 (m, 8H, CH_2), 0.29 (3H, CH_3). ^{13}CNMR (δ, DMSO-d6): 11.5, 18.4, 25.7, 28.1, 41.3, 41.3, 111.5, 118.4, 130.9, 131.8, 135.4, 138.4, 159.2, 163.0. Elemental Analysis for $C_{13}H_{16}N_2O$: C, 72.21; H, 7.40; N, 13.88; O, 7.4.

3.2.9 | 3-(ethyl imino) indolin-2-one (3i)

Brown solid. Yield 80%, m.p. 142–143°C; IR (KBr) cm^{-1}: 3,349.51 (NH), 3,472.90 (NH), 1,638.51 (CO, CN), 1,382.23 (C═C). ^{1}HNMR (δ, DMSO-d6): 7.01 (1H, s, NH), 6.92 (1H, t, Ar), 6.33 (1H, t, Ar), 7.74 (1H, d, Ar), 7.01 (1H, d, NH), 2.49 (2H, q, CH_2), 1.0305 (3H, t, CH_3). ^{13}CNMR (δ, DMSO-d6):11.5, 59.2, 111.5, 118.4, 130.9, 131.8, 135.5, 138.4, 159.2, 163.0. MS (ESI, 70 eV) *m/z* (%): 188.09 (100), 189.10 (11.9). Elemental Analysis for $C_{11}H_{12}N_2O$: C, 68.93; H, 5.71; N, 17.23; O, 9.19.

3.3 | Target and ligand preparation

In order to find out the interactions mode of designed molecules over MAO-B enzyme, Maestro Molecular Modeling platform (version 11.5) by Schrödinger, LLC was used.[43] Initially, the crystal structures of the five human MAO-B enzyme were retrieved from the Protein Data Bank (PDB: 1oja, 2v5z, 2byb, 2vz2, and 2c67 (http://www.rcsb.org).[11,40,44–46] These pdb IDs were selected based on criteria like; highest resolution (Å), being related to *Homo sapiens* specious, wild type with no modified residue, and the existence of co-crystalized ligand, which related to the FDA approved drugs. As the prosthetic group and the co-factors are not directly involved in MAO-B inhibition, they totally removed before docking investigation. Except several ordered water molecules in the MAO-B active site, which bridge the receptor important residues by the way of H-bonds, and conserve among other specious,[47] the rest of the water molecules removed from the enzymes crystallographic structures. The 2D structures of all the synthesized compounds were drawn in Marvin 15.10.12.0 program (http://www.chemaxon.com)[48] and converted into pdb file. The Protein Preparation Wizard[49] and the LigPrep[50] module were used to prepare protein and ligands structure properly.

3.4 | IFD protocol

The IFD (flexible docking) was carried out using Glide software (Schrödinger LLC 2018) to predict accurate concomitant structural movements, including side-chain (χ angles) or backbone (Cα) conformational changes or both during ligand binding at the active site of the MAO-B enzyme.[51] The energy minimized human MAO-B/safinamide complex was subjected for IFD studies as it has the highest resolution among the other pdb structures. At the active site of MAO-B the safinamide binding was used to generate the grid for IFD calculation. The maximum 20 poses with receptor and ligand van der Waals radii of 0.7 and 0.5 Å, respectively, considered. Residues within 5 Å of the safinamide at the active site were refined followed by side-chain optimization. Structures whose Prime energy is more than 30 kcal/mol are eliminated based on extra precious Glide docking. The energetically favorable IFD complexes were obtained for all compounds and the best poses based on IFD Score were selected for MM-GBSA and analysis.

3.5 | Prime MM-GBSA

The ligand binding energies (ΔG_{Bind}) were calculated for each synthesized and MAO-B inhibitors using molecular mechanics/generalized born surface area (MM-GBSA) modules (Schrödinger LLC 2018)[52] based on the following equation;

$$\Delta G_{\text{Bind}} = E_{\text{Complex}} - \left[E_{\text{Receptor}} + E_{\text{Ligand}}\right]$$

where ΔG_{Bind} is the calculated relative free energy, which includes both ligand and receptor strain energy. E_{Complex} is the MM-GBSA energy of the minimized complex, and E_{Ligand} is the MM-GBSA energy of the ligand after removing it from the complex and allowing it to relax. E_{Receptor} is the MM-GBSA energy of relaxed protein after separating it from the ligand. The MM-GBSA calculation was performed based on the best pose structure obtained from IFD complexes.

3.6 | Molecular dynamic (MD) simulation

Molecular simulations of this study were performed using the Desmond v5.3 using Maestro interface (from Schrödinger 2018-4 suite) [53]. We evaluated the stability of the best MM-GBSA compound and compared their perturbation with the standard inhibitor.

In order to build the system for MD simulation, the protein-ligand complexes were solvated with SPC explicit water molecules and placed in the center of an orthorhombic box of appropriate size in the Periodic Boundary Condition. Sufficient counter-ions and a 0.15 M solution of NaCl were also utilized to neutralize the system and to simulate the real cellular ionic concentrations, respectively. The MD protocol involved minimization, pre-production, and finally production MD simulation steps. In the minimization procedure, the entire system was allowed to relax for 2,500 steps by the steepest descent approach. Then the temperature of the system was raised from 0 to 300 K with a small force constant on the enzyme in order to restrict any drastic changes. MD simulations were performed via NPT (constant number of atoms, constant pressure, that is, 1.01325 bar and constant temperature, that is, 300 K) ensemble. The Nose-Hoover chain method was used as the default thermostat with 1.0 ps interval and Martyna-Tobias-Klein as the default barostat with 2.0 ps interval by applying isotropic coupling style. Long-range electrostatic forces were calculated based on Particle-mesh-based Ewald approach with the cut-off radius for columbic forces set to 9.0 Å. Finally, this system was subjected to the production of MD simulations for 20 ns for each protein-ligand complex. During the simulation every 1,000 ps of the actual frame was stored. The dynamic behavior and structural changes of the systems were analyzed by the calculation of energy and the RMSD. Subsequently, the energy-minimized structure calculated from the equilibrated trajectory system was evaluated for investigation of each ligand-protein complex interaction.

3.7 | In silico ADME properties of synthesized compounds

The important pharmacokinetic properties of the synthesized compounds, which represent drug- likeness, metabolism, cell permeation, and bioavailability, were calculated with QikProp module of Schrodinger.[54]

3.8 | Cell viability assay

As toxicity is one of the filtering stage for drug candidate, in preclinical phases, cytotoxicity assays performed on new drug candidate to select more safe and appropriate drugs.[55] Based on ISO recommendation (10993-5, 2009), NIH/3T3 is a good choice for evaluation of cytotoxic potential of candidate drugs.[56] In addition to NIH/3T3 (murine embryonic fibroblast) as a normal cell line, we also examined the effects of the synthesized substances on breast cancer cells (MCF-7). After culturing in RPMI 1640 medium, cells were seeded in 96-well plates

(1 × 104 cells per well). After 24 hr, fresh medium containing different concentrations of synthesized compounds were added at concentrations between 0.1 and 50 μM. At the end of exposure time (24 and 48 hr), supernatant removed and 20 μl of MTT solution (5 mg/ml) was added to each well and incubated. After 4 hr, formazan crystals were dissolved in 100 μl DMSO and optical density was measured with plate reader at 570 and 690 nm. The cell viability was presented as a percentage of the control group.

4 | CONCLUSIONS

The current study involved synthesis, molecular dynamic, ADME prediction, and in vitro cytotoxicity evaluation of 3-imino isatin derivatives as the potential MAO-B inhibitors.

Based on IFD and MM-GBSA study, all of the synthesize compounds have higher free binding energy than isatin (as a reversible noncovalent MAO-B inhibitor). In addition, compounds **3b**, **3c**, **3g**, **3h**, **3i** have higher free binding energy than selegiline, which proposed that isatin analogs have good binding affinity for active site of MAO-B enzyme. Among them compound **3h** with the highest free binding energy adopts an extended conformation spanning from the flavin ring to the entrance of the substrate cavity.

According to compound **3h** bounding-state, Ile199 adopts a conformation in which its side chain positioned in the "open" conformation so the two active site cavities of MAO-B fused and formed a single space, which abled the compound extending to the MAO-B entrance cavity space.

This finding proposed that N_1-alkylated-3-imino isatin could be proposed as new reversible inhibitor that would occupy both cavities of MAO-B active site.

From consideration of the data presented in this paper, we propose that the synthesized compounds pose over the MAO-B active site like as isatin and selegiline, the two known MAO-B inhibitors. In addition, based on Lipinski rule and in silico ADME calculation they pose acceptable drug profiling.

In addition, the designed compounds showed neither cytotoxicity toward normal tissue cells nor cancerous one, which is one of important safety character for any drug candidate.

ACKNOWLEDGMENTS

The authors gratefully acknowledge technical supports of the project by the Islamic Azad University, Science and Research Tehran branch.

ORCID

Javad Azizian https://orcid.org/0000-0002-1392-0274

REFERENCES

[1] M. B. H. Youdim, Y. S. Bakhle, *Br. J. Pharmacol.* **2006**, *147*, S287e.
[2] M. B. H. Youdim, D. Edmondson, K. F. Tipton, *Nat. Rev. Neurosci.* **2006**, *7*, 295.
[3] A. Hald, J. Lotharius, *Exp. Neurol.* **2005**, *193*, 279.
[4] M. Bortolato, K. Chen, J. C. Shih, *Adv. Drug Deliv. Rev.* **2008**, *60*, 1527.
[5] A. Bolasco, S. Carradori, R. Fioravanti, *Expert Opin. Ther. Pat.* **2010**, *20*, 909.
[6] S. Mandel, O. Weinreb, T. Amit, M. B. H. Youdim, *Brain Res. Rev.* **2005**, *48*, 379.
[7] E. Bonaiuto, A. Milelli, G. Cozza, V. Tumiatti, C. Marchetti, E. Agostinelli, C. Fimognari, P. Hrelia, A. Minarini, M. L. Di Paolo, *Eur. J. Med. Chem.* **2013**, *70*, 88.
[8] S. Carradori, R. Silvestri, *J. Med. Chem.* **2015**, *17*, 6717.
[9] R. G. Fariello, *Neurotherapeutics* **2007**, *4*, 110.
[10] F. Hubálek, C. Binda, A. Khalil, M. Li, A. Mattevi, N. Castagnoli, D. E. Edmondson, *J. Biol. Chem.* **2005**, *280*, 15761.
[11] C. Binda, M. Li, F. Hubalek, N. Restelli, D. E. Edmondson, A. Mattevi, *PNAS.* **2003**, 19, *100*, 9750.
[12] E. M. Van der Walt, E. M. Milczek, S. F. Malan, D. E. Edmondson, N. Castagnoli, J. J. Bergh, J. P. Petzer, *Bioorg. Med. Chem. Lett.* **2009**, *19*, 2509.
[13] C. I. Manley-King, J. J. Bergh, J. P. Petzer, *Bioorg. Med. Chem.* **2011**, *19*, 261.
[14] C. M. Silva, D. L. Silvaa, L. V. Modolo, R. B. Alves, M. A. Resende, C. V. B. Martin, A. Fátima, *J. Adv. Res.* **2011**, *2*, 1.
[15] H. Azizian, Z. Mousavi, H. Faraji, M. Tajik, K. Bagherzadeh, P. Bayat, A. Shafiee, A. Almasirad, *J. Mol. Graph. Model.* **2016**, *67*, 127.
[16] S. N. Pandeya, P. Yogeeswari, D. Sriram, E. De Clercq, C. Pannecouque, M. Witvrouw, *Chemotherapy* **1999**, *45*, 192.
[17] S. N. Pandeya, D. Sriram, G. Nath, E. De Clercq, *Eur. J. Med. Chem.* **2000**, *35*, 249.
[18] M. Varma, S. N. Pandeya, K. N. Singh, J. P. Stables, *Acta Pharm.* **2004**, *54*, 49.
[19] S. N. Pandeya, D. Sriram, G. Nath, E. De Clercq, *Arzneimittel-Forschun* **2000**, *50*, 55.
[20] S. N. Pandeya, P. Yogeeswari, D. Sriram, G. Nath, *Bull. Chim. Farm.* **1998**, *137*, 321.
[21] S. N. Pandeya, D. Sriram, G. Nath, E. De Clercq, *Farmaco.* **1999**, *54*, 624.
[22] M. F. Abo-Ashour, W. M. Eldehna, R. F. George, M. M. Abdel-Aziz, M. M. Elaasser, N. M. Abdel Gawad, A. Gupta, S. Bhakta, S. M. Abou-Seri, *Eur. J. Med. Chem.* **2018**, *160*, 49.
[23] S. A. Imam, R. S. Varma, *Experientia* **1975**, *31*, 1287.
[24] R. S. Varma, I. A. Khan, J. Polish, *Pharmacol. Pharm.* **1977**, *29*, 549.
[25] S. N. Pandeya, D. Sriram, G. Nath, E. De Clercq, *Indian J. Pharm. Sci.* **1999**, *61*, 358.
[26] R. S. Varma, W. L. Nobles, *J. Pharm. Sci.* **1975**, *64*, 881.
[27] G. S. Reddy, K. A. Hossain, J. S. Kumar, B. Thirupataiah, R. K. Edwin, V. B. Giliyaru, R. C. Hariharapura, G. G. Shenoy, P. Misraa, M. Pal, *RSC Adv.* **2020**, *10*, 289.

[28] R. S. Varma, W. L. Nobles, *J. Med. Chem.* **1967**, *10*, 972.
[29] S. P. Singh, S. K. Shukla, L. P. Awasthi, *Curr. Sci.* **1983**, *52*, 766.
[30] J. C. Logan, M. P. Fox, J. M. Morgan, A. M. Makohon, C. J. Pfau, *J. Gen. Virol.* **1975**, *28*, 271.
[31] T. Aboul-Fadl, H. A. Abdel-Aziz, M. K. Abdel-Hamid, T. Elsaman, J. Thanassi, M. J. Pucci, *Molecules* **2011**, *16*, 7864.
[32] S. J. Tantry, G. Degiacomi, S. Sharma, L. Jena, A. Narayan, S. Guptha, G. Shanbhag, S. Menasinakai, M. Mallya, D. Awasthy, G. Balakrishnan, P. Kaur, D. Bhattacharjee, C. Narayan, J. Reddy, C. N. N. Kumar, R. Shandil, F. Boldrin, N. Dinesh, *Bioorg. Med. Chem. Lett.* **2015**, *25*, 3234.
[33] M. A. Borad, M. N. Bhoi, S. K. Rathwa, M. S. Vasava, H. D. Patel, C. N. Patel, H. A. Pandya, E. A. Pithawala, J. J. Georrge, *Interdiscip. Sci. Comput. Life Sci.* **2018**, *10*, 411.
[34] N. Nami, D. Zareyee, M. Ghasemi, A. Asgharzadeh, M. Forouzani, S. Mirzad, S. M. Hashemi, *J. Sulfur. Chem.* **2017**, *38*, 279.
[35] M. Farooq, Z. M. Almarhoon, N. A. Taha, A. A. R. Baabbad, M. A. Al-Wadaan, A. El-Faham, *Biol. Pharm. Bull.* **2018**, *41*, 350.
[36] J. Azizian, M. K. Mohammadi, O. Firuzi, N. Razzaghi-asl, R. Miri, *Med. Chem. Res.* **2011**, *21*, 3730.
[37] J. F. M. da Silva, S. J. Garden, A. C. Pinto, *J. Braz. Chem. Soc.* **2001**, *12*, 273.
[38] J. A. Erickson, M. Jalaie, D. H. Robertson, R. A. Lewis, M. Vieth, *J. Med. Chem.* **2004**, *47*, 45.
[39] J. W. M. Nissink, C. Murray, M. Hartshorn, M. L. Verdonk, J. C. Cole, R. Taylor, *Proteins Struct. Funct. Genet.* **2002**, *49*, 457.
[40] C. Binda, J. Wang, L. Pisani, C. Caccia, A. Carotti, P. Salvati, D. E. Edmondson, A. Mattevi, *J. Med. Chem.* **2007**, *50*, 5848.
[41] M. Li, C. Binda, A. Mattevi, D. E. Edmondson, *Biochemistry* **2006**, *45*, 4775.
[42] J. Azizian, H. Fallah-Bagher-Shaidaei, H. Kefayati, *Synth. Commun.* **2003**, *33*, 789.
[43] Schrödinger Release 2018-4, *Maestro*, Schrödinger, LLC, New York, NY **2018**.
[44] L. De Colibus, M. Li, C. Binda, A. Lustig, D. E. Edmondson, A. Mattevi, *PNAS* **2005**, *102*, 12684.
[45] E. M. Milczek, D. Bonivento, C. Binda, A. Mattevi, I. A. McDonald, D. E. Edmondson, *J. Med. Chem.* **2008**, *51*, 8019.
[46] C. Binda, F. Hubalek, M. Li, Y. Herzig, J. Sterling, D. E. Edmondson, A. Mattevi, *J. Med. Chem.* **2005**, *48*, 8148.
[47] C. Binda, F. Huba′lek, M. Li, Y. Herzig, J. Sterling, D. E. Edmondson, A. Mattevi, *J. Med. Chem.* **2004**, *47*, 1767.
[48] ChemAxon ChemAxon Marvin was used for drawing, displaying and characterizing chemical structures, substructures and reactions, Marvin 15.10.12.0 (version number), **2015**, ChemAxon http://www.chemaxon.com.
[49] Schrödinger Release 2018-4, *Schrödinger Release 2018-4 Protein Preparation Wizard; Epik*, Schrödinger, LLC, New York, NY **2018** Impact, Schrödinger, LLC, New York, NY, 2018; Prime, Schrödinger, LLC, New York, NY, 2018.
[50] Schrödinger Release 2018-4, *LigPrep*, Schrödinger, LLC, New York, NY **2018**.
[51] Schrödinger Release 2018-4, *Induced Fit Docking Protocol; Glide*, Schrödinger, LLC, New York, NY **2018** Prime, Schrödinger, LLC, New York, NY, 2018.
[52] Schrödinger Release 2018-4, *Prime; MM-GBSA*, Schrödinger, LLC, New York, NY **2018**.
[53] Schrödinger Release 2018-4, *Desmond Molecular Dynamics System*, D. E. Shaw Research, New York, NY **2018** Maestro-Desmond Interoperability Tools, Schrödinger, New York, NY, 2018.
[54] Schrödinger Release 2018-4, *QikProp*, Schrödinger, LLC, New York, NY **2018**.
[55] G. Turan-Zitouni, W. Hussein, B. N. Sağlık, A. Tabbi, B. Korkut, *Molecules* **2018**, *23*(1), 113.
[56] International Organization for Standardization, *Biological Evaluation of Medical Devices-Part 5: Tests for in vitro Cytotoxicity ISO-10993-5*, 3rd ed., International Organization for Standardization, Geneva, Switzerland **2009**.

SUPPORTING INFORMATION

Additional supporting information may be found online in the Supporting Information section at the end of this article.

How to cite this article: Ahmadi S, Azizian H, Azizian J. Imino isatin derivatives; synthesis, in silico molecular dynamic study over monoamine oxidase B, ADME prediction, and in vitro cytotoxicity evaluation. *J Chin Chem Soc*. 2021; 1–14. https://doi.org/10.1002/jccs.202000170